Biochimica et Biophysica Acta, 408 (1975) 306–318
© Elsevier Scientific Publishing Company, Amsterdam – Printed in The Netherlands

BBA 47012

ON THE NATURE OF THE IRON SULFUR CLUSTER IN A DEUTERATED ALGAL FERREDOXIN

RUSSELL E. ANDERSON[a], W. RICHARD DUNHAM[a], RICHARD H. SANDS[a], ALAN J. BEARDEN[b] and HENRY L. CRESPI[c]

[a]*Biophysics Research Division, Institute of Science and Technology, University of Michigan, Ann Arbor, Mich. 48105,* [b]*Donner Laboratory, University of California, Berkely, Calif. 94720 and* [c]*Chemistry Division, Argonne National Laboratory, Argonne, Ill. 60439 (U.S.A.)*

(Received May 9th, 1975)

SUMMARY

A protonated and a completely deuterated two-iron algal ferredoxin from *Synechococcus lividus* have been studied by optical, electron paramagnetic resonance, electron-nuclear double resonance, proton magnetic resonance and Mossbauer spectroscopies; temperature dependent magnetic susceptibility measurements are reported as well. These studies have confirmed the electron localized model of the active center in the two-iron ferredoxins, as previously deduced from studies of spinach ferredoxin, have yielded much more precise spectroscopic parameters for this center, and have thus greatly increased the confidence in this model.

INTRODUCTION

The two iron, two labile sulfur plant type ferredoxins from spinach and parsley (and to a lesser extent those from *Pseudomonas putida* and pig adrenal cortex) have been well characterized by optical [1], EPR, NMR [2–4], ENDOR [5], Mossbauer [6], and magnetic susceptibility [7] measurements (see also a recent review [8]). These measurements show that in both oxidation states there is an antiferromagnetic exchange interaction between the electron spins of the two iron atoms. In the oxidized state the two nearly equivalent iron atoms are both high spin ferric ($S = 5/2$) resulting in diamagnetism below 77 °K and paramagnetism which increases with temperature above 77 °K. Upon single electron reduction, the ferredoxin displays Curie $S = 1/2$ paramagnetism below 77 °K and paramagnetism greater than Curie above 77 °K, resulting from the antiferromagnetic exchange interaction between a high spin ferric and a high spin ferrous iron. The ferrous iron atom is in a rhombically distorted tetrahedral ligand field (probably consisting of two labile and two cysteine sulfur atoms) with the reducing electron in a d_{z^2} orbital. These results have been summarized [4] and shown to support the basic exchange coupled spin model proposed [9] to explain the spinach ferredoxin EPR data. The recent model compound studies of Holm et al. [10] have confirmed this structural model for the active site.

Although spinach ferredoxin is the most extensively studied ferredoxin, two components of the ferrous hyperfine tensor were undetermined due to intense, overlapping proton ENDOR resonances and hence these parameters were relatively free in the Mossbauer simulations. This made it difficult to prove uniqueness and made the determinations of the quadrupole interaction tensors tenuous. In order to obtain more reliable Mossbauer simulations (and parameters) on which nearly all interpretations are based, the above measurements were repeated on algal ferredoxin from *Synechococcus lividus* grown on a totally deuterated medium. The elimination of the proton ENDOR signals permitted the determination of all three components of the hyperfine tensors for both iron atoms in the reduced state.

The results of EPR, ENDOR, Mossbauer, PMR and magnetic susceptibility are presented here, but when the results are identical to those of spinach ferredoxin the reader is referred to the previous references [1–8] for a more complete discussion.

MATERIALS

The growth of the fully deuterated algae (*Synechococcus lividus*) [11], the extraction of the ferredoxin [12], and the iron exchange procedures [5] have been described elsewhere; optical, EPR and activity measurements [13] show that the reconstituted protein is identical to the native protein. The only changes required in the preparative procedures for the deuterated proteins are that the reconstitution must be performed in deuterated (potassium phosphate) buffers and the DE-52 and P-60 columns must both be equilibrated in the deuterated buffers [13]. The G-75 column used in previous preparations was not used. For algal ferredoxin the purity ratio is typically $A_{420nm}/A_{276nm} = 0.65$. The ENDOR samples are approximately 4 mM in 0.3 ml and were reduced in the EPR tubes using a 0.5 M dithionite solution in 1 M potassium phosphate buffer. A three-fold excess of dithionite was added, the solution is stirred for 10 s, then frozen and stored in liquid nitrogen. Approximately 1 μmol of protein was used for the Mossbauer and ENDOR measurements and 10–15 μmol were used for the magnetic susceptibility measurements.

The EPR spectrometer is a modified commercial Varian V-4500 while the homemade ENDOR spectrometer [5] and Mossbauer spectrometer are described elsewhere [6].

RESULTS

The above model deduced for the active center of the two-iron ferredoxins from spinach and parsley, is concluded here as well. All of the data have been interpreted in terms of this model.

Magnetic susceptibility

The variation with temperature of the static magnetic susceptibility of fully protonated algal ferredoxin was measured on an Iizuka-Kotani [14] torsion balance and establishes the existence of an iron-iron antiferromagnetic exchange interaction essentially identical to that observed for spinach ferredoxin [7]: The oxidized protein is diamagnetic at low temperatures and becomes increasingly paramagnetic at temperatures above 77 °K; although these data alone cannot determine the iron spin states,

the two states must have the same spin and can be simulated for $S_1 = S_2 = 5/2$ (see Mossbauer results) and $J = -185\ cm^{-1}$ [13] where the spin-exchange interaction is given by $\mathscr{H} = -2J\vec{S}_1 \cdot \vec{S}_2$.

The reduced protein demonstrates approximately Curie $S = 1/2$ paramagnetism at 77 °K but paramagnetism greater than Curie at higher temperatures [13]. This again indicates an exchange interaction between spins whose magnitudes differ by 1/2 and can be simulated with $J = -115\ cm^{-1}$, $S_1 = 5/2$, and $S_2 = 2$ (spin states determined by Mossbauer spectroscopy). If the first excited electronic state of the high spin ferrous iron lies $430\ cm^{-1}$ (see Mossbauer results) above the ground d_{z^2} state, then the reduced ferredoxin susceptibility is fit with $J = -98\ cm^{-1}$.

EPR

EPR was attempted on both oxidized and reduced algal ferredoxins. No EPR signal was observed in the oxidized protein, consistent with the diamagnetism observed at low temperature (see magnetic susceptibility above) while the EPR spectrum of reduced algal ferredoxin [13] is essentially identical to that of reduced spinach ferredoxin [8]. The EPR for protonated algal ferredoxin can be simulated with $S_{eff} = 1/2$ (consistent with the magnetic susceptibility for reduced ferredoxin), $g_{x,y,z} = 1.88$, 1.96, 2.05, and the half widths at half maximum $L_{x,y,z} = 22$, 13, and 9.5 gauss. The large anisotropic linewidths, characteristic of many iron sulfur proteins, differ at 9 versus 35 GHz by an amount linear (within 5 %) with the polarizing magnetic field. Such behavior can be represented in the spin Hamiltonian by a distribution of g-values ("g-strain") presumably due to protein conformational heterogeneity ([8] and Strong, L., Palaith, D. and Sands, R. H., in preparation).

The presence of iron at the reducing site is demonstrated by reconstitution of the ferredoxin with ^{57}Fe ($I = 1/2$) whose magnetic moment interacts with the reducing electron, but the resulting 20 % linewidth increase at g_z allows determination of neither the magnitude of the hyperfine interaction, nor the number of iron atoms involved. The presence of proton hyperfine interactions is indicated by a 10 % linewidth decrease at g_z for fully deuterated relative to fully protonated algal ferredoxin.

ENDOR

The anisotropy of the g-tensor allows one to select molecules of a particular orientation or set of orientations to study by EPR by sitting at a fixed magnetic field, H_0. If this EPR absorption is partially saturated it is possible by monitoring the intensity of that absorption to detect the nuclear magnetic resonance of nuclei coupled to the electron for those molecules having this selected set of orientations. By employing different values of H_0 and keeping track of the corresponding molecular orientations selected, it is possible to determine not only the principal values of the hyperfine (A) tensor but the relative orientation of the A-tensor with respect to the g-tensor for each of the nuclei involved. This is the method of ENDOR. The reader should see ref. 5 for details.

To unequivocally identify the signals due to ^{57}Fe, ENDOR spectra were recorded for the ^{57}Fe and ^{56}Fe reconstituted protein and the latter spectra subtracted from the former.

(1) *Ferric.* Since no ENDOR resonances are observed above 20 MHz for reduced native (i.e., ^{56}Fe, $I = 0$) algal ferredoxin, those seen in Fig. 1 for ^{57}Fe

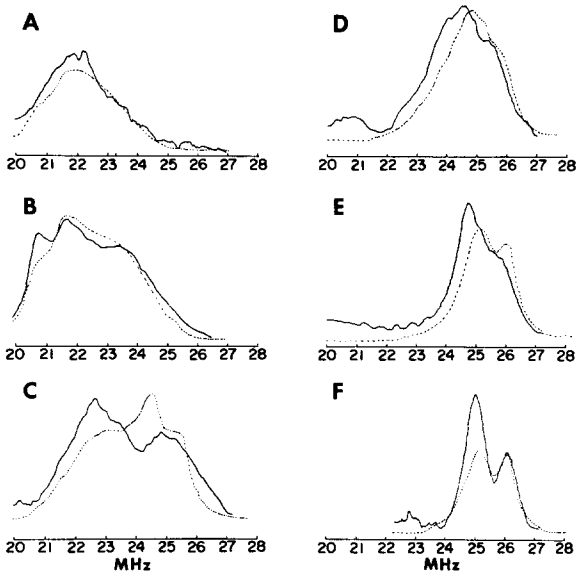

Fig. 1. Experimental (solid curve) and simulated (dashed curve) ferric ENDOR spectra of reduced ^{57}Fe reconstituted algal ferredoxin. $T = 13$ °K. Microwave power = 7 mW. (A) $H_0 = H_z$, (B) $H_0 = H_z + 30$ gauss, (C) $H_0 = H_z + 120$ gauss, (D) $H_0 = H_x - 80$ gauss, (E) $H_0 = H_x$, (F) $H_0 = H_x + 60$ gauss, where $H_x = h\nu/g_x\beta$, $H_y = h\nu/g_y\beta$, $H_z = h\nu/g_z\beta$, with $g_{x,y,z}$ taken from Table I.

($I = 1/2$) reconstituted ferredoxin are due to an electron-nuclear hyperfine interaction between at least one iron atom and the unpaired electron. A resolved ENDOR doublet centered at 25.7 MHz ($A'_{eff}/2$) and split by twice the nuclear Zeeman frequency ($\approx$ 1 MHz) occurs at $H_x + 60$ gauss where predominantly only a single protein orientation satisfies the EPR and ENDOR resonant conditions; the accompanying computer simulation fixes $A'_x = 51.6$ MHz. H_z, like H_x, selects a unique protein orientation, but the observation of a doublet at $H_z + 30$ gauss and not at H_z in this case indicates [5] that the hyperfine tensor is rotated 25–35° about the g_x axis with $A'_z = 42$ MHz. Reduced doublets are not observed at H_y and other intermediate field positions because many protein orientations satisfy the resonance conditions; A'_y is determined by computer simulation to be 50 ± 2 MHz. (The above hyperfine parameters are primed to indicate that they refer to the rotated A-tensor principal axis frame.)

The simulations (dashes lines) in Fig. 1 were computed using the hyperfine values in Table I under the very simplistic model [5, 12] of the relaxation times and transition probabilities being independent of orientation. Such a model should be good whenever only a small number of orientations are present; but when, as in Fig. 1C, there are a large number of orientations undergoing EPR and hence ENDOR the fit is not good nor should it be expected to be. We have not attempted to refine this model because we do not know how the relaxation times depend on orientation.

The nearly isotropic hyperfine interaction can be assigned (see Mossbauer results) to a high spin ferric atom, which is undergoing spin-exchange with another iron atom.

TABLE I

MOSSBAUER PARAMETERS FOR OXIDIZED AND REDUCED ALGAL FERREDOXIN

Where

$$\eta \equiv \frac{\frac{\partial^2 V}{\partial x^2} - \frac{\partial^2 V}{\partial y^2}}{\frac{\partial^2 V}{\partial z^2}}$$

and the values of the hyperfine tensor components are quoted in MHz and in equivalent gauss field splittings produced at the electron.

A. Oxidized ferredoxin			
I.S./Pt (mm/s)	-0.13 ± 0.02		
Q.S. (mm/s)	$0.55 \& 0.83 \pm 0.04$		2 sites
η	0.5 ± 0.3		
B. Reduced ferredoxin	*Ferric*		*Ferrous*
a. High temperature			
I.S./Pt (mm/s)	-0.15 ± 0.02		0.13 ± 0.02
Q.S. (mm/s)	0.60 ± 0.02		-2.69 ± 0.02
b. Low temperature			
I.S./Pt (mm/s)	-0.20 ± 0.02		0.07 ± 0.02
Q.S. (mm/s)	0.60 ± 0.02		-3.20 ± 0.1
η	-0.3 ± 0.3		0.0 ± 0.2
g_x*		1.89	
g_y		1.96	
g_z		2.05	
A_x (MHz)	$-51.6+0.2$ -0.4		$13.0+0.1$ -0.5
A_x (electron gauss)	$-19.5+0.1$ -0.2		$4.9+0.1$ -0.2
A_y (MHz)	-50.0 ± 2		15.0 ± 1.0
A_y (electron gauss)	-18.2 ± 0.7		5.4 ± 0.4
A_z (MHz)	$-42.0+0.2$ -0.5		36.5 ± 0.5
A_z (electron gauss)	$-14.6+0.1$ -0.3		12.7 ± 0.2

* g-values from EPR.

(2) *Ferrous.* ENDOR spectroscopy below 20 MHz for the ferredoxins [5] demonstrates many resolved proton resonances and a baseline increasing at low frequency due to components of the radio frequency field parallel to the dc field and perhaps unresolved nitrogen ENDOR. These proton resonances precluded the observation of two of the three principal axis hyperfine components in the ferrous ENDOR resonances in spinach ferredoxin [5] which are observed in the fully deuterated algal ferredoxin.

As for spinach ferredoxin [5], Fig. 2A shows that for $H_0 = H_z$, an ENDOR intensity difference (^{57}Fe–^{56}Fe) occurs at 17.5 MHz distinct from the above mentioned ferric resonance at 22 MHz. The difference spectrum at H_z is replotted in Fig. 2D together with a computer simulation. The distribution has a full width at

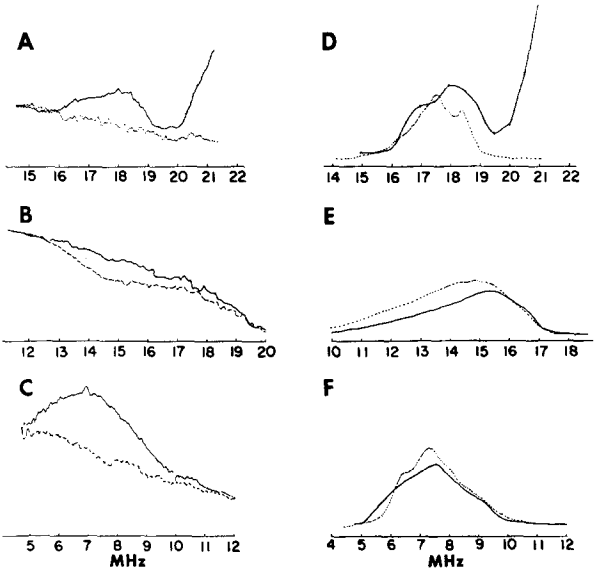

Fig. 2. Ferrous ENDOR spectra of reduced algal ferredoxin. $T = 10$ °K. Microwave power = 14 mW. (A), (B), and (C) are experimental ^{57}Fe (solid) and ^{56}Fe (dashed) reconstituted ferredoxin spectra at $H_0 = H_z$, H_z+60 gauss and H_x respectively. (D), (E), and (F) are hand plotted experimental differences (solid) and computer simulated (dashed) spectra for $H_0 = H_z$, H_z+60 gauss, and H_x respectively.

half maximum of 2.5 MHz and is due principally to A_z hyperfine resonances while the skewing to the low frequency side is due to contributions from molecules whose g_z axis is not quite oriented parallel to H_z. The simulation uses $A_z = 36.5$ MHz, a value within the larger experimental errors for spinach, parsley, adrenodoxin, putidaredoxin, and protonated algal ferredoxin. At H_x a single rf sweep range encompasses the difference signal (Fig. 2C, F), a 2.5 MHz wide distribution peaked and centered at 6.5 MHz and establishing $A_x = 13.0\ ^{+0.1}_{-0.5}$ MHz. This resonance has never been observed in a protonated ferredoxin. See Table I for the total range of A_x and A_z values permitted by the data.

For applied fields greater than H_z, the ferric distribution (see above) moves to high frequency and the new ferrous resonances skew toward low frequency. Whereas the zero difference signal begins at 16 MHz at H_z, it begins at 15.5 MHz at H_z+30 gauss, and at 12.5 MHz at H_z+60 gauss (Fig. 2B, E). The maximum of the distribution moves more slowly, having reached 15.5 MHz at H_z+60 gauss relative to 18.5 MHz at H_z. This broadening occurs because many orientations, hence many A_{eff} values, are sampled when the applied field is not set to H_z, but yet the nearest principal hyperfine value still dominates. At H_z+90 gauss the difference intensity is very small (10 % of the background) due to the great width (4 MHz) of the distribution; at this field the iron difference signal extends from 9.5 to 17.5 MHz.

Since at H_y the instrument rf sweep range cannot span the A_y distribution, three overlapping ranges were used. The lowest range (3–7 MHz, with the relative gains set for zero difference at 3 MHz, an assumption justified by the A_x measurement) shows that the difference signal begins at 5 MHz. The intermediate field scan (4.5–

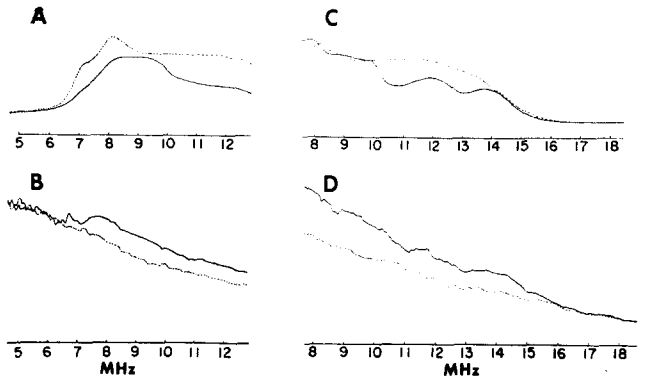

Fig. 3. Ferrous ENDOR spectra of reduced algal ferredoxin. T = 10 °K. Microwave power = 14 mW at $H_0 = H_y$. (B) and (D) are experimental spectra for ^{57}Fe (solid) and ^{56}Fe (dashed) reconstituted ferredoxin. (A) and (C) are hand plotted difference (solid) and computer simulated (dashed) spectra.

13 MHz, Fig. 3A, B) confirms this behavior and shows a resonance which is essentially flat from 8 MHz to the end of the sweep range. The high frequency portion (7.6 to 20 MHz) of the distribution, shown in Fig. 3C is obtained by setting the amplifier gain for zero difference signal at 19 MHz; this is justified by the movement of the distribution from A_z as noted above. With these gain adjustments, it was found that the zero difference extends from 15.5 MHz to 19 MHz (Fig. 3C, D); above 19 MHz it is the ferric iron which contributes to the difference. Below 14 MHz the distribution is essentially flat to the bottom of the range at 7.6 MHz; the largest signal difference in this region is approximately 15 % of the background. Since many orientation angles satisfy the H_y resonant condition the observed difference signal requires a computer simulation to show that $A_y = 15 \pm 1$ MHz.We were unable to observe any effects which suggested that these A-tensor principal axes were rotated with respect to the g-tensor axes.

The hyperfine parameters deduced from the computer simulations are summarized in the lower portion of Table I. The assignment of the respective tensors to a ferric and ferrous atom is made from the Mossbauer results to be discussed later.

(3) *Proton ENDOR.* The H_x ENDOR spectrum of fully protonated algal ferredoxin in Tris-Cl buffer is shown in Fig. 4A. This spectrum begins at 7.5 MHz where the intensity is due to the effects discussed previously. The 10–20 MHz segment of Fig. 4A shows six pairs of semi-resolved proton lines, centered at the free proton frequency (14.65 MHz at H_x) and split by their hyperfine value. Note that the intensities of each pair need not be equal. None of these resolved resonances disappears if the sample is freeze-dried and soaked in ^2H_2O, but a change in the overall shape suggests that some unresolved protons are exchangeable.

When the algae is grown on a fully deuterated medium, extracted in protonated phosphate buffers, transferred to Tris-Cl buffer, twice freeze-dried and taken up with ^2H_2O, the ENDOR spectrum in Fig. 4B is obtained; the relative gain in Fig. 4B is about five times that of Fig. 4A. A deuterated sample extracted in totally deuterated phosphate buffers shows only the sloping low frequency baseline at all fields (Fig. 4D).

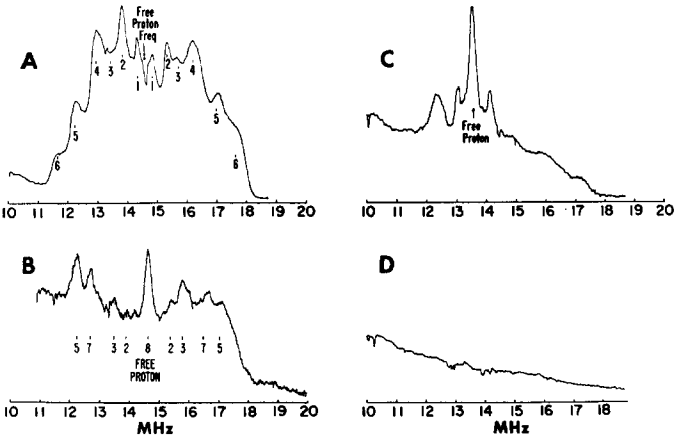

Fig. 4. Proton ENDOR spectra of reduced algal ferredoxin. $T = 20$ °K. Microwave power = 7 mW. (A) Fully protonated ferredoxin at H_x, (B) and (C) "fully" deuterated ferredoxin extracted in protonated Tris-Cl buffers, twice freeze-dried and soaked in ^2H_2O for 1 week, at $H_0 = H_x$ and H_z respectively. (D) fully deuterated ferredoxin extracted in deuterated phosphate buffers.

The resonances seen in Fig. 4B and C but not in 4D show that protons exchange on during protein isolation but do not totally re-exchange, even if soaked in ^2H_2O for one week. These protons are rapidly exchanged, however, in the apoprotein when the Fe reconstitution is performed in deuterated buffers. Notice also that protons 2, 3, and 5 appear in both Fig. 4A and 4B. The weakly coupled protons, 8, exchange quickly except for those due to the nonexchangeable Tris protons. These Tris protons are weakly coupled to the unpaired spin and the intensity of the signal is related to the Tris concentration. There are no strongly coupled, rapidly exchanging protons.

These proton data are unfortunately, not readily amenable to interpretation due principally to the difficulty in following the ENDOR resonance frequency dependence on EPR field position. Attempts to use exchange kinetics to identify these protons proved unsuccessful. From the proton ENDOR linewidths one can obtain the electron T_2, the 0.5 MHz ENDOR linewidths indicating that the EPR spectrum is a summation of lines 0.15 gauss wide.

Mossbauer results

The best-fit parameters for the Mossbauer data for algal ferredoxin are summarized in Table I and should be compared with the nearly identical spinach ferredoxin data [6]. As that same reference contains the necessary experimental, theoretical and interpretive details only the summarized results and changes in simulations due to new ENDOR data will be presented here.

The results for the low temperature (4.2 °K) Mossbauer spectroscopy of oxidized algal ferredoxin are shown in Fig. 5A and B. The low field data ($H = 580$ gauss) is approximately simulated by a single quadrupole pair (Q.S. = −0.13 mm/s), if the linewidth is increased from the instrumental linewidth of 0.15 mm/s to 0.2 mm/s. A better fit (Fig. 5A) is achieved with two quadrupole pairs ($Q.S._1 = 0.83$ mm/s and $Q.S._2 = -0.55$ mm/s), each with the same isomer shift and 0.17 mm/s linewidths.

The low field data is identical at 4.2 °K and 77 °K [13] indicating that over this

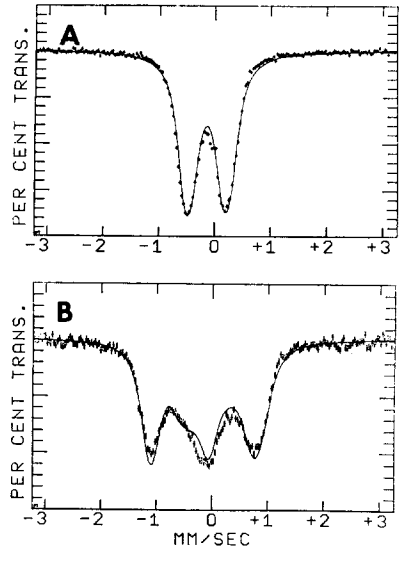

Fig. 5. Experimental (+ + +) and computer simulated (solid) Mossbauer spectra for oxidized algal ferredoxin. (A) $T = 4$ °K, $H = 580$ gauss, (B) $T = 4$ °K, $H = 46$ kgauss.

range, Q.S. is independent of temperature.

At high field the nuclear Zeeman interactions become important resulting in the additional structure observed in Fig. 5B. The simulations assume the quadrupole splittings and isomer shift from the low field data while eta and the signs of the Q.S. are varied for the best fit. Positive quadrupole splittings and eta = 0.5 are best for both the single and two quadrupole pair interpretations, the latter giving the better fit. (Fig. 5B).

The Mossbauer results indicate that the oxidized protein has two slightly non-equivalent iron atoms, each with a small positive Q.S. and linewidth slightly greater than the inherent instrumental linewidth. This latter fact suggests a distribution of iron environments due to protein microheterogeneity also indicated by the EPR "g-strain".

Reduced ferredoxin

The Mossbauer effect spectra for high temperature (250 °K) reduced algal ferredoxin is shown in Fig. 6A ($H = 580$ gauss) and Fig. 6B ($H = 46$ kgauss). These high temperature spectra are characteristic of two iron sites with nonequivalent quadrupole splittings [6], and no average internal fields; they demonstrate that one iron ("Site I"), has nearly the same Q.S. (0.60 mm/s) and isomer shift (−0.15 mm/s) as one of the iron atoms in the oxidized protein while the other iron ("Site II") has a very large quadrupole splitting (2.69 mm/s) and an isomer shift of +0.13 mm/s. The above data fit the line positions but the best lineshape fits require a Site I/Site II amplitude ratio of 0.6/0.5 (explainable by incomplete protein reduction) and linewidths of 0.2 and 0.17 mm/s for Site I and Site II, respectively.

Since Q.S. is nearly the same for the oxidized protein and Site I of the reduced

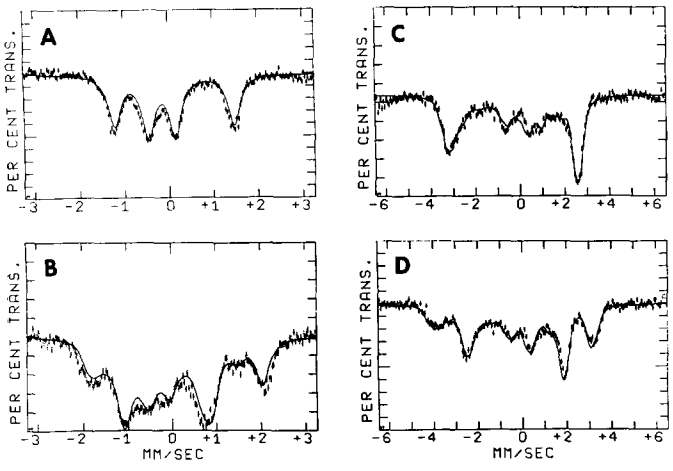

Fig. 6. Experimental (+++) and calculated (solid) Mossbauer spectra for reduced algal ferredoxin. (A) $T = 250$ °K, $H = 580$ gauss; (B) $T = 250$ °K, $H = 46$ kgauss; (C) $T = 4$ °K, $H = 580$ gauss; (D) $T = 4$ °K, $H = 46$ kgauss.

protein, the sign and eta from the oxidized protein are assumed for the high temperature high field simulations. The sign of Q.S. for Site II is found to be negative and an eta equal to zero is marginally preferred over an eta equal to one. The large negative Q.S. together with the isomer shift immediately establishes the Site II as high spin ferrous iron ($S_2 = 2$) with the reducing electron in a ground state d_{z^2} orbital [6]. The inequality of the Site I Q.S. in the reduced state to either of the oxidized quadrupole splittings shows that the Site I electric field is slightly altered by the reducing electron, but the oxidation state of the Site I iron is unchanged upon reduction.

At low temperatures (4.2 °K) electron relaxation rates are slowed to the point where any paramagnetic internal fields have lifetimes greater than the nuclear excited state lifetime (which is greater than the nuclear precession times in these fields) and result in resolved hyperfine structure. This effect is observed in the low field (580 gauss, Fig. 6C) and high field 46 kgauss (Fig. 6D) Mossbauer data. When the applied field is small with respect to the internal fields but large enough to align the spin moments, the two spin states will exhibit identical Mossbauer spectra [6] as shown in Fig. 6C. The calculated simulation assumes the magnitudes of the hyperfine tensors from the ENDOR data (Table I), the EPR g-values, and the Site I Q.S. and eta from the high temperature Mossbauer data. Site I (ferric) Q.S. is assumed to be independent of temperature because of its similarity to the temperature independent Q.S. for oxidized ferredoxin; Q.S. for Site II is a free parameter and is found to increase from -2.69 mm/s at high temperature to -3.2 mm/s at low temperature. This behavior indicates [6] that an excited state with a smaller or opposite Q.S. has a finite Boltzmann population at high temperature and is consistent with the first electron excited state lying 430 cm^{-1} above the ground state. The rotation of the Site I hyperfine tensor relative to the g-tensor, as indicated by the ENDOR results, measurably improves the fit at both high and low fields; since no data is available for the quadrupole orientation, it was assumed coincident with the g-tensor.

The low temperature high field spectra consist of four spectra (weighted by the ratio of their Boltzmann factors which at 4.2 °K and 46 kgauss applied field is 3.3), two each for $m_s = -1/2$ and $m_s = 1/2$. The simulation requires that the Site I ground state ($m_s = -1/2$) hyperfine field be aligned antiparallel to the applied field while the ferrous, Site II, ground state hyperfine field is aligned parallel and its eta is approximately zero. This behavior is positive proof [6] that the high spin ferrous ion ($S_2 = 2$) is antiferromagnetically coupled to a high spin ferric ion ($S_1 = 5/2$), because that is the only way that the internal hyperfine field of the $S = 2$ ferrous ion can be aligned parallel to the applied field (positive effective A). The near equality of the isomer shifts and quadrupole splittings of the iron atoms in the oxidized state to those of Site I iron in the reduced state then indicates that both iron atoms in the oxidized state are high-spin ferric. This model of antiferromagnetically coupled high-spin iron atoms is consistent with the susceptibility data as discussed previously.

All the parameters used in the Mossbauer simulations are summarized in Table I.

High resolution NMR results

Fig. 7 displays the PMR spectra of contact shifted protons of oxidized and reduced ferredoxin (in ^2H_2O) from *S. lividus*. All spectra were recorded at 20 °C, 220 MHz, and 20 kHz modulation frequency by continuous wave repetitive scanning on the Varian instrument in the Chemistry Division at Argonne National Laboratories. The results are quite similar to those obtained with spinach ferredoxin by Salmeen and Palmer [3] and Poe et al. [2]. With oxidized ferredoxin (top trace) a broad resonance representing 6 to 9 protons was observed at 34 ppm (downfield from trisilyltetradeuterio sodium propionate) while Salmeen and Palmer [3] observed a

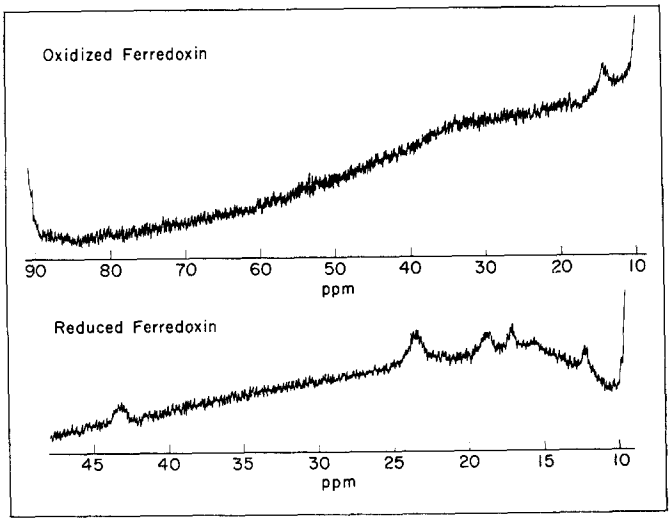

Fig. 7. Signal averaged CW proton magnetic resonance spectra of oxidized (top) and reduced (bottom) algal ferredoxin showing contact shifted lines. Each spectrum is the result of 2048 accumulated scans. Scan rates were 800 Hz/s (oxidized ferredoxin) and 400 Hz/s (reduced ferredoxin) at high power levels. Spectra of the reduced ferredoxin obtained at 100 and 200 Hz/s gave the same result.

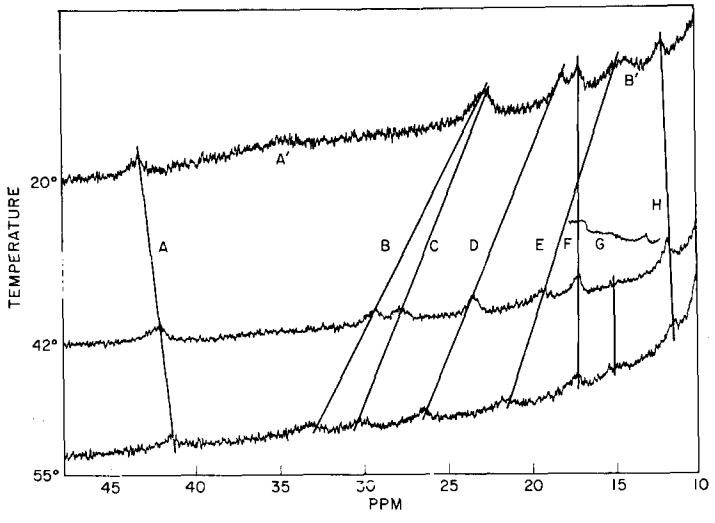

Fig. 8. 200 MHz NMR spectra of reduced algal ferredoxin at 20, 42, and 55 °C.

similar line at 37 ppm. Reduced ferredoxin (bottom trace) shows lines at 12.4, 16.0, 17.3, 18.9, and 23.6 ppm which are analogous to resonances obtained (at 220 MHz) by Poe et al. [2] with spinach ferredoxin. The line at 43 ppm (bottom trace) is analogous to the line observed (at 60 MHz) by Salmeen and Palmer [3] with spinach ferredoxin. Within the limits of our instrumentation, we found no other contact shifted resonances.

Fig. 8 shows the temperature dependences of the proton lines observed in the reduced protein. These temperature dependences are in accord with the previous interpretations [3, 4] for spinach ferredoxin and serve to confirm the antiferromagnetic coupling between the high-spin iron atoms in the reduced state of this algal protein as well.

CONCLUSION

The use of fully deuterated protein has allowed the experimental determination of the three principal hyperfine components for both the ferric and ferrous atoms in *S. lividus* ferredoxin. This work has reduced markedly the uncertainty in the Mossbauer parameters and has confirmed the active site electron-localized model [9, 4] for the plant type ferredoxins:

(a) The oxidized state contains two high spin ferric atoms antiferromagnetically coupled ($J = -185\ cm^{-1}$) to give a net $S = 0$, diamagnetism below 77 °K. These two iron sites appear not to be equivalent.

(b) The $S = 1/2$ (at low temperature) reduced state consists of one high spin ferric antiferromagnetically coupled ($J = -115\ cm^{-1}$) to a high spin ferrous whose first excited state lies $430\ cm^{-1}$ above the ground d_{z^2} state. The ferric Mossbauer parameters are only slightly altered upon protein reduction.

While the ligands are thought to be tetrahedrally coordinated labile and

cysteine sulfurs, ENDOR shows at least seven classes of strongly coupled protons, none of which are rapidly exchanged; four classes of protons are however exchangeable in the apoprotein. PMR shows at least six contact shifted protons whose temperature dependences reconfirm the antiferromagnetic exchange interaction; correlation of PMR and proton ENDOR lines has not been possible. Solvent (e.g., water and Tris) protons are weakly coupled but the net effect of all the proton hyperfine interactions is a 10 % increase in EPR linewidth. The 10–20 gauss linewidths in the deuterated protein must arise from a distribution of lines each of which has a width less than 0.15 gauss (from ENDOR linewidth) and which seem to be due to microheterogeneity in the iron environments; similar effects are observed in the Mossbauer linewidths.

The more complete measurements possible here with algal ferredoxin have greatly increased the confidence in the localized-electron, exchange-coupled model first proposed by Gibson et al. [9] to explain the spinach EPR data.

ACKNOWLEDGEMENTS

We wish to thank Drs. Takashi Yonetani and Mamoru Tamora of the Department of Physical Biochemistry, Johnson Research Foundation, University of Pennsylvania for the magnetic susceptibility measurements. We also thank Professor Graham Palmer for his advice and assistance. This work was supported by NIH Research Grant GM-12176 and Argonne National Laboratory. The principal author (REA) gratefully acknowledges fellowship support by NIH Training Grant GM-1355.

REFERENCES

1 Eaton, W. A., Palmer, G., Fee, J. A., Kimura, T. and Lovenberg, W. (1971) Proc. Natl. Acad. Sci. U.S. 68, 3015–3020
2 Poe, M., Phillips, W. D., Glickson, J. D., McDonald, C. C. and San Pietro, A. (1971) Proc. Natl. Acad. Sci. U.S. 68, 68–71
3 Salmeen, I. and Palmer, G. (1972) Arch. Biochem. Biophys. 150, 767–773
4 Dunham, W. R., Palmer, G., Sands, R. H. and Bearden, A. J. (1971) Biochim. Biophys. Acta 253, 373–384
5 Fritz, J., Anderson, R., Fee, J. A., Palmer, G., Sands, R. H., Tsibris, J. C. M., Gunsalus, I. C., Orme-Johnson, W. H. and Beinert, H. (1971) Biochim. Biophys. Acta 253, 110–133
6 Dunham, W. R., Bearden, A. J., Salmeen, I. T., Palmer, G., Sands, R. H., Orme-Johnson, W. H. and Beinert, H. (1971) Biochim. Biophys. Acta 253, 134–152
7 Palmer, G., Dunham, W. R., Fee, J. A., Sands, R. H., Iizuka, T. and Yonetani, T. (1971) Biochim. Biophys. Acta 245, 201–208
8 Sands, R. H. and Dunham, W. R. (1975) Q. Rev. Biophys. 7, 443–504
9 Gibson J. F., Hall, D. O., Thornley, J. H. and Whatley, F. R. (1966) Proc. Natl. Acad. Sci. U.S. 56, 987–990
10 Mayerle, J. J., Frankel, R. B., Holm, R. H., Ibers, J. A., Phillips, W. D. and Weiher, J. F. (1973) Proc. Natl. Acad. Sci. U.S. 70, 2429–2433
11 Katz, J. J. and Crespi, H. L. (1966) Science 151, 1187–1194
12 Crespi, H. L. and Katz, J. J. (1972) Preparation of Deuterated Proteins and Enzymes in Methods in Enzymology (Hirs, C. H. W. and Timasheff, S. N. eds), Vol. XXVI, Enzyme Structure, Part C, Academic Press
13 Anderson, R. E. (1972) Thesis, University of Michigan, University Microfilms No. 73–11032
14 Iizuka, T. and Kotani, M. (1969) Biochim. Biophys. Acta 181, 275–286